



Pattern Speeds and Galaxy Morphology

R. Buta¹ and X. Zhang²

¹ Department of Physics and Astronomy, University of Alabama, Box 870324, Tuscaloosa, AL 35487 e-mail: rbuta@bama.ua.edu

² Department of Physics and Astronomy, George Mason University, Fairfax, VA 22030, e-mail: xzhang5@gmu.edu

Abstract. The morphology of a disk galaxy is closely linked to its kinematic state. This is because density wave features are likely made of spontaneously-formed modes which are allowed to arise in the galactic resonant cavity of a particular basic disk state. The pattern speed of a density wave is an important parameter that characterizes the wave and its associated resonances. Numerical simulations by various authors have enabled us to interpret some galaxies in terms of high or low pattern speeds. The potential-density phase-shift method for locating corotation radii is an effective new tool for utilizing galaxy morphology to determine the kinematic properties of galaxies. The dynamical mechanism underlying this association is also responsible for the secular evolution of galaxies. We describe recent results from the application of this new method to more than 150 galaxies in the Ohio State University Bright Galaxy Survey and other datasets.

1. Introduction

The pattern speed Ω_p of a spiral or bar perturbation is an important physical parameter describing density wave features in galaxies. Although often treated as a free parameter in passive numerical simulations, the pattern speed for a galaxy with a given basic state (described by the radial distribution of its star/gas surface densities, velocity dispersion, and rotation curve) is not arbitrary but is determined by the basic state as part of its spontaneously-formed density wave modal characteristics (Bertin et al. 1989), although interactions between galaxies can temporarily alter some of these characteristics.

The pattern speed of a density wave, together with the galaxy rotation curve, determines the locations of all wave-particle reso-

nances. These resonances affect the shape of nearby periodic orbits, which can lead to the formation of rings (Buta and Combes 1996), and also limit the extent of the patterns themselves (e.g., Contopoulos 1980; Contopoulos & Grosbol 1986). Furthermore, pattern speed, which determines the location of the corotation resonance (CR), also influences the manner in which angular momentum is exchanged with the basic state (Zhang 1998) when the angular momentum flux is being transported outward by the density wave (Lynden-Bell and Kalnajs 1972). This non-uniform angular momentum flux (or the non-zero radial gradient of the flux) leads to the secular morphological evolution of galaxies (Zhang 1996, 1998, 1999). The pattern speed may also influence the lifetime of a pattern (Merrifield et al. 2006).

To gauge connections between pattern speed and galaxy morphology, one can (1) di-

Send offprint requests to: R. Buta

rectly measure pattern speeds or resonance locations and connect observed features to resonances; or (2) compare sequences of numerical simulations with actual galaxies, either through generic modeling or modeling of a specific galaxy. For example, Garcia-Burillo et al. (1993), in modeling M51, state that “The gas response is very sensitive to the [pattern speed]; we obtain a spiral structure similar to what is observed only for a narrow range of Ω_p .” Included in (1) are applications of the Tremaine & Weinberg (1984) continuity equation method (see other papers in this volume), and also our potential-density phase-shift method (section 3), which taps into a more general connection between galaxy morphology and galaxy kinematic features.

2. Pattern Speed and Galactic Rings

Rings are believed to be direct tracers of wave-particle resonances. As noted by Buta and Combes (1996), “rings are a precious tool to measure the pattern speed when the rotation curve is known.” It is worth re-examining models of ringed galaxies to see how Ω_p might affect what we see. The models of Schwarzschild (1981), Simkin et al. (1980), and Byrd et al. (1994) used test-particles to represent gas in analytic, rigidly rotating bar potentials. Salo et al. (1999) also used gaseous test-particles, but in a bar potential inferred from a near-infrared image. Rautiainen & Salo (2000) used n -body simulations to define the bar potential and gaseous test-particles, and were able to find multiple modes. Lin et al. (2008) used hydrodynamical models to study the rings in NGC 6782. All of these models showed that rings are linked to specific orbit resonances in a bar potential. Other interpretations are provided by Regan & Teuben (2004), who describe rings in terms of orbit family transitions rather than resonances, and by Romero-Gomez et al. (2006; see also this volume), who link rings to invariant manifolds of orbits around the equilibrium points of the bar.

Pattern speed can have subtle or major effects on a galaxy’s structure. The effects of Ω_p for a barred galaxy were explicitly studied by Byrd et al. (1994), which confirmed

the theoretically expected correlations between the value of the pattern speed and the type of resonances allowed in a galaxy. Byrd et al. identified “pattern speed domains” defined by the presence or absence of inner resonances, such as the inner Lindblad resonance (ILR) and the inner 4:1 ultraharmonic resonance (IUHR). High Ω_p models had corotation (CR) and outer Lindblad resonance (OLR), but not ILR or IUHR. Medium Ω_p domain models had IUHR, CR, and OLR, but not ILR, while lower Ω_p models had all the main resonances. According to the Byrd et al. models, a galaxy possessing an outer ring or pseudoring but no inner or nuclear rings would be a candidate for the high Ω_p domain, while a galaxy having inner and outer rings or pseudorings but no nuclear ring would be a candidate for the medium Ω_p domain. Those galaxies showing three or four possible rings (one or two outer rings, an inner ring, and a nuclear ring) would be candidates for the low Ω_p domain. The domains are nevertheless ambiguous because a galaxy could possess all the main resonances, and not show all the rings because of a lack of gas near some resonances.

Figures 1- 4 compare specific Byrd et al. simulation frames with observed galaxies mostly from Buta & Crocker (1991). These support indirectly the idea of pattern speed domains. The comparisons highlight not only specific effects of Ω_p but also possible effects of morphological evolution (if the sequence is interpreted as a time frame). In Figure 1, ESO 509–98 [type (R₁R₂)SB(s)a], and ESO 365–35 [type (R₂)SAB(l)0/a] are two early-type spirals that strongly resemble high Ω_p Byrd et al. models. Both lack an inner ring or nuclear star formation (Buta & Crocker 1991), which could imply the lack of inner resonances.

Figure 2 shows three galaxies that could be in the medium Ω_p domain in that all have conspicuous inner and outer rings/pseudorings, but lack nuclear rings. The Byrd et al. sequence shows an R₁’ outer pseudoring evolving to an R₂’ outer pseudoring, and the three illustrated galaxies bear a strong resemblance to the sequence. Figure 3 shows a pair of low Ω_p domain frames that again show an R₁’ pseudoring

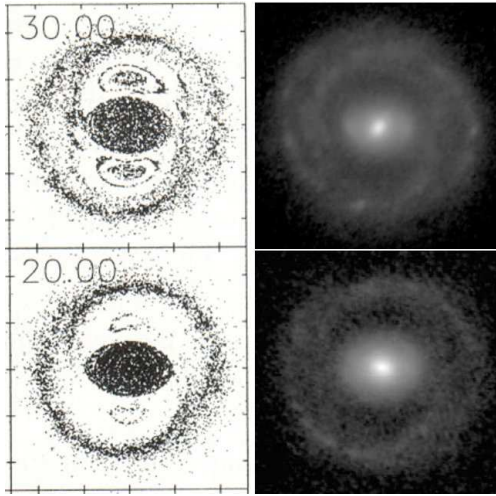


Fig. 1. These simulated outer pseudoring patterns at left (top: $\Omega_p = 0.27$; bottom: $\Omega_p = 0.22$, where Ω_p is dimensionless) occur at the OLR and were produced in high Ω_p domain models by Byrd et al. (1994). The number at upper left shows the number of bar rotations. The galaxies at right are: ESO 509–98 (top) and ESO 365–35.

evolving to an R'_2 ring. The frames include both nuclear rings and inner rings. The two matching galaxies have similar outer and inner rings, but also from color index maps are known to have a nuclear ring or blue nucleus, suggesting the existence of an ILR. Figure 4 shows a strong resemblance between the galaxy NGC 1566 and a frame from the lowest Ω_p Byrd et al. model. Instead of a nuclear ring, the model shows a bright inner spiral, and both galaxy and model have an R'_1 outer pseudoring.

Although the generic Byrd et al. (1994) models match very well the morphology of some normal galaxies, the models are limited in allowing only a single pattern speed. The Rautiainen & Salo (2000; see also Rautiainen & Salo 1999) models were more sophisticated in that they allowed investigation of multiple modes. These authors highlighted a case where a bar might appear misaligned with an inner ring because the spiral/ring has a different pattern speed from the bar. ESO 565–11 very much resembles such a model (Figure 5). However, the general alignment of bars and inner rings (e.g., Buta 1995) would seem to ar-

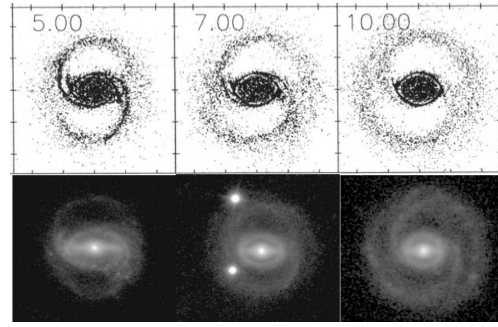


Fig. 2. A sequence of frames from Byrd et al. (1994) for medium $\Omega_p = 0.10$, covering 5-10 bar rotations. The comparable galaxies are (left to right): ESO 575–47, ESO 426–2, and ESO 577–3. All three have conspicuous inner and outer rings/pseudorings, but lack nuclear star formation based on color index maps from Buta & Crocker (1991).

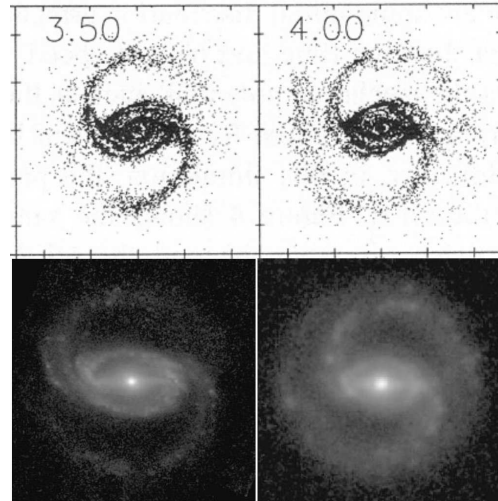


Fig. 3. Two frames from a low Ω_p domain Byrd et al. sequence having $\Omega_p = 0.06$, at 3.5 and 4.0 bar rotations. The model shows inner, outer, and nuclear gas rings/pseudorings. The comparable galaxies are: ESO 437–67 (left) and ESO 325–28. The former has a small blue nuclear ring while the latter has a blue nucleus (Buta & Crocker 1991).

gue that, in many ringed galaxies at least, the bar and the ring/spiral could have the same or a similar pattern speed.

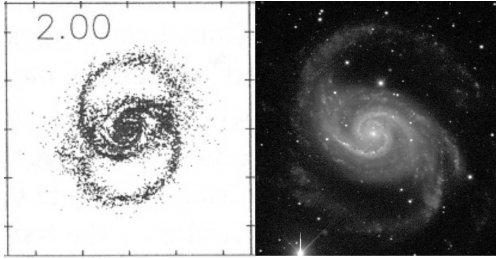


Fig. 4. A frame from the lowest Ω_p sequence of Byrd et al., showing that a conspicuous spiral develops inside a large oval region, with an R_1' outer pseudoring breaking from its ends. The galaxy NGC 1566 bears a strong resemblance to this frame.

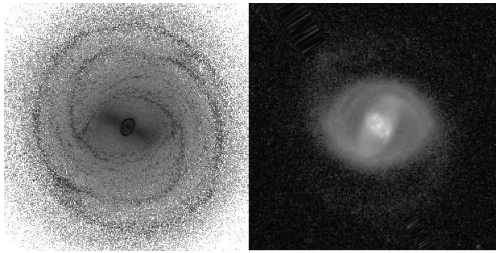


Fig. 5. The misaligned bar-inner ring galaxy ESO 565-11 is a strong candidate for a multiple Ω_p system, according to the models of Rautiainen & Salo (2000), one of which is shown at left.

Rautiainen et al. (2004) found that an interesting pattern may develop between the inner and outer 4:1 resonances in a barred galaxy: a symmetric $m=4$ spiral. Figure 6 shows a numerical model where the potential has been derived from an H -band image and evolved mostly with a maximum disk/bulge in the inner regions. This model shows a four-armed pattern confined between the inner and outer 4:1 resonances that strongly resembles what is seen in ESO 566-24. A similar conclusion was reached by Treuthardt et al. (2008) for the spiral morphology of NGC 1433.

This section shows that relatively simple numerical simulations can account for many aspects of barred galaxy morphology even though most of these simulations are passive in assuming a static bulge/disk potential forcing and do not allow the bar to evolve. Also, except for Rautiainen & Salo (1999, 2000), these models had assumed a single pattern

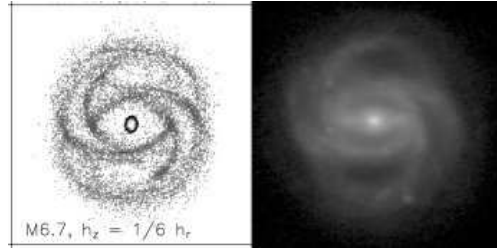


Fig. 6. A four-armed barred spiral model (left) from Rautiainen et al. (2004) as compared to a V -band image of ESO 566-24.

speed, and thus are of limited applicability. The method we describe next allows us to probe galaxy structure in a more in-depth manner.

3. The Potential-Density Phase-Shift Method for Locating Corotation Radii

There are numerous methods for measuring pattern speeds and locating resonances in galaxies independent of rings (for, example, see other papers in this volume). The potential-density phase-shift method uses the zero-crossings of the azimuthal phase difference between the wave perturbation density and the potential implied by that density, to locate corotation radii in galaxies (Figure 7). The method was conceived by Zhang (1996, 1998, 1999) and first applied to real galaxies by Zhang & Buta (2007). The phase difference leads to a torque applied by the spiral potential on the disk density (see eq. 1 of Zhang & Buta 2007). This torque can lead to a slow secular evolution of the disk surface density across the entire galactic disk, not just at the main resonances as advocated by Lynden-Bell & Kalnajs (1972). Over a Hubble time, a substantial bulge can be built up by this process. Note that the method only works if a given pattern is skewed. Non-skewed patterns will not show phase-shifts.

One requirement for the successful application of this method is that wave modes in galaxies are quasi-stationary, which allows the morphological features to track kinematic characteristics. In such a state, CR would exactly correspond to positive-to-negative (P/N)

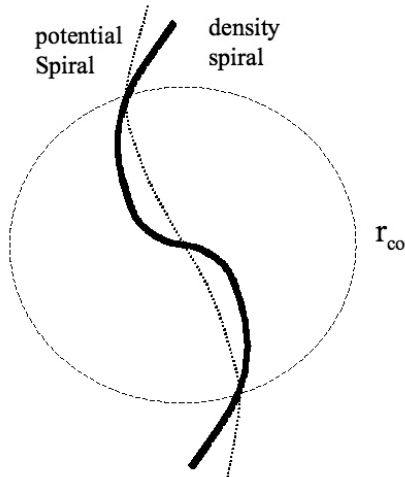


Fig. 7. Schematic showing the phase difference between potential and density in a spiral galaxy, and how the difference changes sign across corotation (labeled r_{co}).

zero crossings in graphs of potential-density phase differences versus radius (Zhang 1996, 1998). Inside CR, the density spiral is ahead of the potential spiral, while outside CR, the density spiral lags the potential spiral (Figure 7). If multiple patterns with independent Ω_p are present, then we will see multiple P/N crossings. Negative-to-positive (N/P) crossings appear to delineate the extent of the modes which may terminate at their OLR.

To calculate the phase-shifts, we use red or near-infrared images to infer the gravitational potentials, assuming a constant mass-to-light ratio. Ideally, images in the wavelength range 1.6-4.5 μ m are best, but even red continuum, Cousins I -band, or SDSS i -band images are useful, depending on Hubble type. When the method is applied to many galaxies, we note the following trends: (1) multiple P/N crossings are common, implying nested, multiple patterns; (2) the crossings are generally not arbitrary but seem closely connected to resonant features; (3) there is evidence for decoupling of nested patterns, i.e., a bar and spiral may initially grow together but eventually their pattern speeds decouple.

The phase-shift distributions $\phi_0(r)$ versus radius r , normalized to the radius, $r_o(25)$, of the $\mu_B=25.00$ mag arcsec $^{-2}$ isophote corrected for galactic extinction and tilt from RC3 (de Vaucouleurs et al. 1991), are shown for three strongly-barred galaxies in Figure 8. These are based on K_s -band images from Buta et al. (2008). The first example, NGC 986, also has a strong spiral breaking from the bar ends and shows only a single P/N crossing (arrow) in its phase-shift plot. It could be a genuine case of a “bar-driven” spiral, where the two features have grown together and share the same pattern speed. The second example, NGC 613, shows two crossings in the bar region (plus one near the center), which we suggest indicates that the inner part of the bar is decoupling from the outer spiral. In the third example, NGC 175, the spiral and the bar are fully decoupled and each has a well-defined P/N crossing. Both NGC 175 and 986 satisfy the “rule” that the bar extends no further than its CR (Contopoulos 1980).

Figure 9 shows the interesting case of NGC 1300, which has a well-defined skewed bar and two strong P/N crossings corresponding to the smaller and larger circles on the image. The main P/N crossing associated with the bar lies inside the prominent bar ansae, while the main outer crossing is clearly associated with the outer spiral arms. We conclude: (1) Only the inner portion of the spiral arms associated with the bar is a bar-driven spiral; the outer portion appears to break off at the location of the strong N/P crossing between the two CRs and is likely to be a distinct mode; and (2) the prominent bar spills over its CR radius by more than 30%. We argued in Zhang & Buta (2007) that cases where $r(CR) < r(bar)$ are not necessarily due to image or method noise, but could be genuine cases violating Contopoulos’s finding that a bar can extend no further than its own CR, a result which was based on passive orbit analysis in the potential of a non-skewed bar. Support for our finding is that, in order for the SWING mechanism (Toomre 1981) to amplify spontaneously-formed bars, a bar cannot terminate cleanly at its CR without a corresponding wave portion outside CR to receive the transmitted wave. This outer portion could

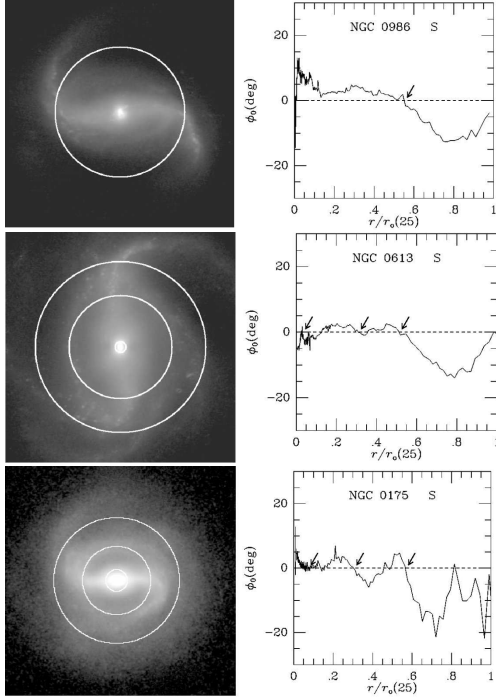


Fig. 8. K_s -band images and phase-shift distributions of three galaxies: (top) NGC 986; (middle) NGC 613; and (bottom) NGC 175. The arrows on the phase-shift plots show the main P/N crossings, and hence the implied CR radii. The circles superposed on the images show these radii.

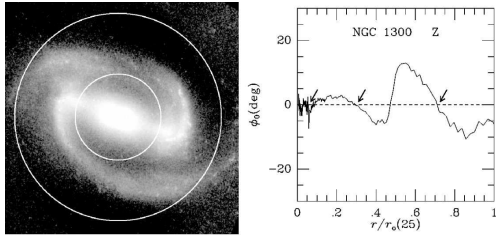


Fig. 9. K_s -band image and derived phase-shift distribution for NGC 1300. The circles superposed on the image show the two larger derived CR radii.

be in the form of a bar-driven spiral, but could also be in the form of a slightly-twisted long bar which forms a continuation of the inner bar.

Do phase-shift distributions provide any support for the implications from test-particle and other numerical models of barred spirals,

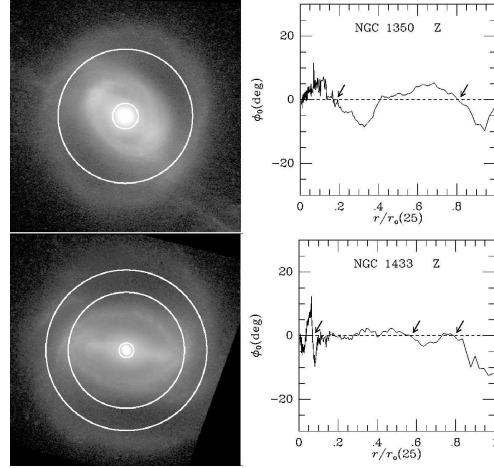


Fig. 10. Red continuum images (Crocker et al. 1996) and phase-shift distributions for NGC 1350 (upper frames) and NGC 1433 (lower frames). The circles show the derived CR radii (arrows). The phase-shift distribution of NGC 1433 shows additional weak crossings in the bar region that are likely significant.

as outlined in section 2? That is, do outer rings lie outside CR and inner rings inside CR? The phase-shift distribution of double-ringed galaxy NGC 1350 (Figure 10, upper frames) shows two P/N crossings corresponding to the two circles superposed on the image. The smaller circle seems associated with a pattern inside the bar, while the larger circle lies between the inner and outer pseudorings. Thus, in this case there is some support for the findings from the numerical models. The case of NGC 1433 (Figure 10, lower frames) is more complicated. This galaxy shows two major P/N crossings, one surrounding the ends of the main bar and inner ring, and the other passing between the outer pseudoring and the extended oval connected with the inner ring. Interestingly, the radii of these two inferred CRs are very similar to the radii of the IUHR and CR derived by Treuthardt et al. (2008) from a single Ω_p numerical simulation of NGC 1433. Our conclusion is that the bar and oval/spiral of NGC 1433 do not have the same Ω_p .

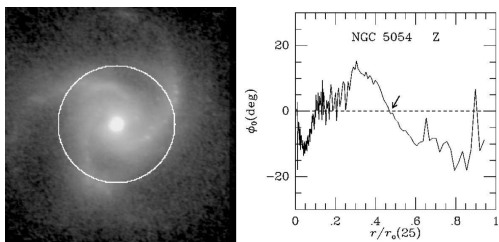


Fig. 11. *H*-band image of NGC 5054 (Eskridge et al. 2002) and corresponding phase-shift distribution. The circle superposed on the image corresponds to the single P/N crossing (arrow).

Do phase-shift distributions support the idea of Contopoulos & Grosbol (1986) and Patsis & Kaufmann (1999) that the main part of a grand-design spiral extends no further than the IUHR, which is typically $2/3$ the radius of CR? Figure 11 shows the phase-shift distribution of the three-armed spiral NGC 5054. Only a single major P/N crossing is found, and it corresponds to the circle shown on the image. This circle passes through the middle of the spiral, and suggests that the pattern most likely extends to the OLR, not the IUHR. We have found several other cases of a grand design spiral pattern extending well beyond CR in Zhang & Buta (2007) and Buta & Zhang (2008).

4. Phase-Shift Results from Analysis of OSUBGS Images

Buta & Zhang (2008) have derived phase-shift distributions of 153 Ohio State University Bright Galaxy Survey (OSUBGS) galaxies based on deprojected *H*-band images from the analysis of Laurikainen et al. (2004), who also compiled estimates of bar radii. With our estimates of bar CR radii from the phase-shift plots, we have investigated the ratio $\mathcal{R} = r(\text{CR})/r(\text{bar})$, where $r(\text{CR})$ is the bar CR radius judged by P/N crossings near the bar radius. \mathcal{R} has been linked to the central concentration of the dark matter halo by Debattista & Sellwood (2000), who defined fast bars to have $\mathcal{R} \leq 1.4$ and slow bars to have $\mathcal{R} > 1.4$. Figure 12 shows our estimates of \mathcal{R} for 100 galaxies with what Laurikainen et al. called “Fourier bars,” which are defined by a con-

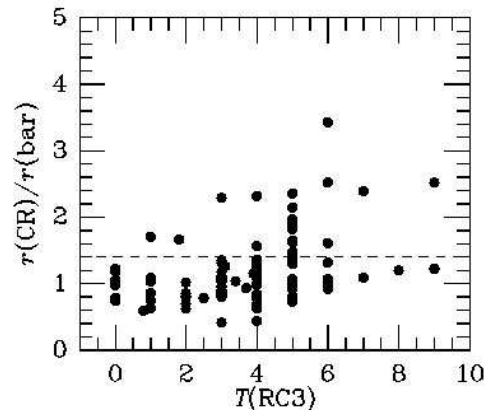


Fig. 12. Type dependence of the ratio of bar corotation radius to bar major axis radius, based on phase-shift determined CR radii and published bar radii from Laurikainen et al. (2004). The dashed horizontal line is the division between fast and slow bars as defined by Debattista & Sellwood (2000).

stant $m=2$ phase, plotted against the revised stage index T from RC3. This shows a type-dependence in the sense that \mathcal{R} averages at 1.01 ± 0.36 for 65 galaxies of type $T=4$ (Sbc) and earlier, and at 1.48 ± 0.62 for 35 galaxies of type $T=5$ (Sc) and later.

How well do CR radii estimated using the potential-density phase-shift method compare with the results of other approaches? Rautiainen et al. (2005, 2008) used numerical simulations to estimate CR radii for 38 OSUBGS galaxies. The idea was to use a near-IR image to estimate the potential, and then evolve a cloud-particle disk in this potential until the cloud morphology matches the *B*-band appearance of the spiral arms. Our approach generally gives smaller values of $r(\text{CR})$ than that of Rautiainen et al. (Figure 13), and we found that one of the reasons for this systematic difference is that the nature of the simulation approach is such that matching *B*-band spiral morphologies often latches the chosen solution onto the Ω_p of the spiral, and not necessarily the Ω_p of the bar. This conclusion was also arrived at independently by Rautiainen et al. (2008). In spite of the differences shown in Figure 13, Rautiainen et al. (2005) found a similar trend of \mathcal{R} with Hubble type.

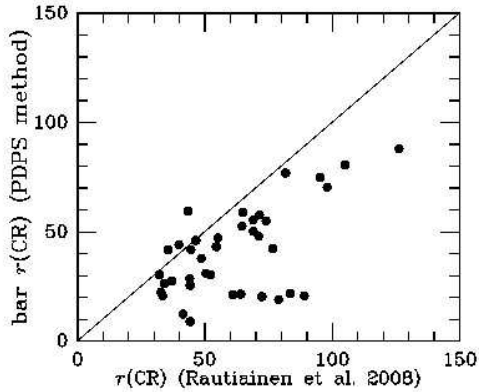


Fig. 13. A graph of bar CR radii estimated from the potential-density phase-shift method versus the CR radii estimated for 38 galaxies by Rautiainen et al. (2008), using the numerical simulation approach.

5. Conclusions

Numerical simulations have been very useful for highlighting the impact of pattern speed on galaxy structure. From comparisons with ringed galaxies, there is a suggestion of the existence of pattern speed domains, where certain major resonances may or may not exist. The potential-density phase-shift method suggests that multiple pattern speeds are common in spiral and barred galaxies. Both bar-driven and non-bar-driven spirals are detected. The method also brings attention to the possibility of “super-fast bars,” where $r(CR) < r(bar)$.

Acknowledgements. We thank E. Laurikainen and J. H. Knapen for some of the images used in this paper. RB acknowledges the support of NSF Grant AST-0507140. Funding for the OSUBGS was provided by NSF grants AST 92-17716 and AST 96-17006, with additional funding from the Ohio State University.

References

- Bertin, G., et al. 1989, *ApJ*, 338, 78
 Buta, R. 1995, *ApJS*, 96, 39
 Buta, R. & Combes, F. 1996, *Fund. Cos. Phys.* 17, 95
 Buta, R. & Crocker, D. 1991, *AJ*, 102, 1715
 Buta, R. & Zhang, X. 2008, submitted to *ApJS*
 Buta, R., et al. 2008, submitted to *AJ*
 Byrd, G., et al. 1994, *AJ*, 108, 476
 Contopoulos, G. 1980, *A&A*, 31, 198
 Contopoulos, G. 1995, *ASP Conf. Ser.* 91, 454
 Contopoulos, G. & Grosbøl, P. 1986, *A&A*, 155, 11
 Crocker, D.i, et al. 1996, *ApJS*, 105, 353
 Debattista, V. & Sellwood, J. 2000, *ApJ*, 543, 704
 de Vaucouleurs, G., et al. 1991, *Third Reference Catalogue of Bright Galaxies*, New York, Springer
 Eskridge, P., et al. 2002, *ApJS*, 143, 73
 Garcia-Burillo, S., et al. 1993, *A&A*, 274, 148
 Laurikainen, E., et al. 2004, *MNRAS*, 355, 1251
 Lin, L.H., et al. 2008, *ApJ*, 684, 1048
 Lynden-Bell, D. & Kalnajs, A. 1972, *MNRAS*, 157, 1
 Merrifield, M., et al. 2006, *MNRAS*, 366, L17
 Patsis, P. & Kaufmann, D. 1999, *A&A*, 352, 469
 Rautiainen, P. & Salo, H. 1999, *A&A*, 348, 737
 Rautiainen, P. & Salo, H. 2000, *A&A*, 362, 465
 Rautiainen, P., et al. 2004, *MNRAS*, 349, 933
 Rautiainen, P., et al. 2005, *ApJ*, 631, L129
 Rautiainen, P., et al. 2008, *MNRAS*, 388, 1803
 Regan, M. & Teuben, P. 2004, *ApJ*, 600, 585
 Romero-Gomez, M., et al. 2006, *A&A*, 453, 39
 Salo, H., et al. 1999, *AJ*, 117, 192
 Schwarz, M. P. 1981, *ApJ*, 247, 77
 Simkin, S., et al. 1980, *ApJ*, 237, 404
 Toomre, A. 1981, in *The Structure and Evolution of Normal Galaxies*, Cambridge Univ. Press, p. 111
 Tremaine, S. & Weinberg, 1984, *ApJ*, 282, L5
 Truthardt, P., et al. 2008, *AJ*, 136, 300
 Zhang, X. 1996, *ApJ*, 457, 125
 Zhang, X. 1998, *ApJ*, 499, 93
 Zhang, X. 1999, *ApJ*, 518, 613
 Zhang, X. & Buta, R. 2007, *AJ*, 133, 2584